

REAL-TIME MEASUREMENT IN SLOW DISPLACEMENT OF THE TUNNEL FLOOR DUE TO DYNAMIC GROUND MOTION AT THE KEKB INJECTOR LINAC

T. Suwada*, Y. Enomoto, K. Kakihara, K. Mikawa, T. Higo, KEK, Tsukuba, Japan

Abstract

A new remote-controllable sensing system in a laser-based alignment system is in progress to evaluate slow dynamic displacement of the tunnel floor in real time at the KEKB injector linac. Based on the recent real-time measurements over six months, we have found that the transverse displacements of the tunnel floor are not negligibly small in comparison with the required alignment tolerance. The cross-correlation analysis shows the positive correlation among the measurement positions on average over the entire linac, except for the two at both ends, while the cross-correlation function varies irregularly during the short term. In this report, the measurement and analysis results are in detail described in slow displacement of the tunnel floor of the KEKB injector linac with a laser-based alignment system.

INTRODUCTION

The Super KEK B-Factory (SKEKB) project [1] is a next-generation B-factory under construction at KEK after the KEKB B-Factory (KEKB) project [2]. The SKEKB is an asymmetric electron-positron collider comprising 4-GeV positron (LER) and 7-GeV electron (HER) rings. The target luminosity of the SKEKB will be 40 times of the peak luminosity of the KEKB. The motivation of the SKEKB is the urgent need to perform high-energy flavor particle physics experiments concerning the CP violation in B mesons [3]. Because the SKEKB is a factory machine, well-controlled operation and high-precision alignment for the accelerator complex are indispensable for maintaining the injection efficiency, stability of the beam collision, and peak luminosity at the maximum.

A laser-based alignment technique is one of the prominent alignment techniques developed for long-distance accelerator complexes. This alignment technique is advantageous as it can not only be applied to initial alignment measurements for long linacs but can also be utilized for regular monitoring of the straightness of the beam line along the entire linac without any interruption during the linac operation. Based on these benefits, dynamic spatial displacements of the tunnel floor along the entire length of the linac due to ground motion can be measured in real time.

Our method is a conventional laser-based alignment technique in which transverse spatial displacements of the accelerator components from a laser-based fiducial line can be measured with quadrant silicon photodiodes (QPDs), where the laser-based fiducial is directly made as a laser

axis by connecting two (or three) fiducial points. A QPD is mounted at a target point, which should be aligned in an accelerator unit, and it is directly irradiated by the laser-based fiducial with a relatively narrow beam width. The central positions at the target can be estimated by measuring the intensity centroid of the laser-based fiducial in the transverse directions on the QPD. Based on this alignment technique, the accelerator units of the linac can be precisely aligned along the laser axis by measuring the transverse displacements from the laser fiducial.

For the purpose in the real-time measurements of the dynamic displacements, two remote-controllable QPDs were installed at the head and middle of the injector linac in summer shutdown of 2014, and seven remote-controllable QPDs were additionally installed in summer shutdown of 2015 at multiple locations near expansion joints of the linac building (see Table 1). After the setup procedure, the real-time measurements of the long-term displacements of the tunnel floor has been started to take data on 7 January 2016. The tunnel floor is located 5.65 m below the earth's surface in which the klystron gallery is situated.

In this report, the consecutively measurement results with a laser-based alignment system are in detail described. Here, the new remote-sensing system and its performance will be reported elsewhere [4].

KEKB INJECTOR LINAC

Here, we briefly describe the components and operation scheme only related to a laser-based alignment system of the injector linac. Figure 1 shows a schematic layout of the KEKB injector linac [5]. It comprises eight sectors (A–C and 1–5), which together constitute two long straight sections. One section is 125 m long and is composed of sectors A and B; the other is 476 m long and is composed of sectors C and 1–5. These two straight sections are connected to a 180° arc section with a circumferential length of 31 m.

Single-bunch electron beams can be generated from a conventional thermionic electron gun (AT gun) and are passed through a pre-injector to attain a pulse width of ~ 10 ps [6]. The electron gun can generate electron beams at maximum charges of 20 nC/bunch and a maximum repetition rate of 50 Hz for positron production. The primary electron beams (~ 10 nC/bunch) can be stably accelerated to 3.3 GeV from the end of the buncher up to a positron production target installed at the front of unit 1-5.

The positrons are captured with a flux concentrator and accelerated up to an energy of 120 MeV using large-aperture S-band accelerating structures [7]. The subsequently positioned normal S-band accelerating structures

* tsuyoshi.suwada@kek.jp

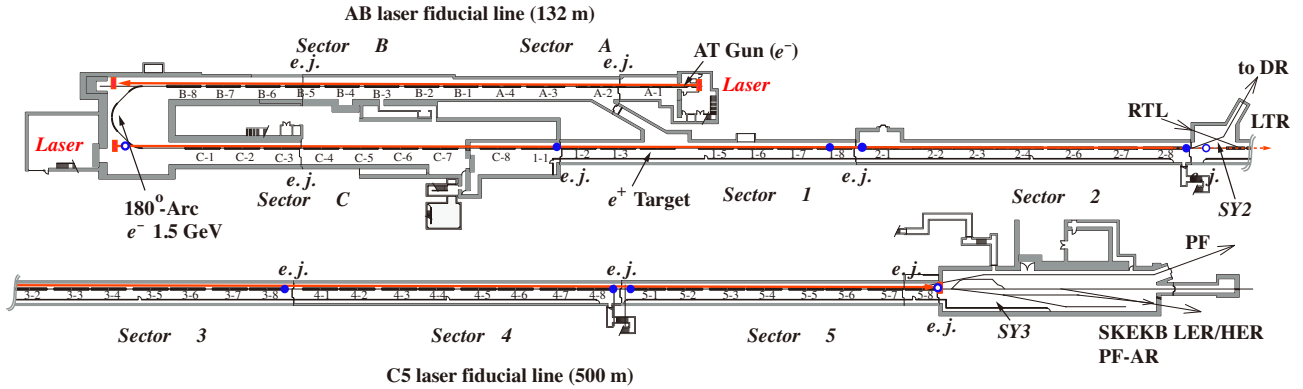


Figure 1: Schematic layout of the KEKB injector linac and laser fiducials for two long straight sections. The abbreviation *e.j.* indicates an expansion joint between the building blocks of the linac. The two arrows (red) show the laser-based fiducials for two long straight sections. The solid circles (blue) represent the remote-controllable QPDs fixed at the accelerator unit and the open circles (blue) represent the reference remote-controllable QPDs fixed at the tunnel floor.

Table 1: Summary table in the locations of the remote-controllable QPDs and expansion joints (*e.j.*) along the injector linac from the laser source. Some measurement results, the maximum norm (r_m) of the displacement vector and the maximum slope (s_r) in the variations in the time traces of the norm, are also summarized depending on the QPD locations.

| QPD | <i>e.j.</i> | L [m] | r_m [mm] | s_r [$\mu\text{m}/\text{day}$] |
|---------|-------------|------------|---------------|---------------------------------------|
| REF1UA | | 1.74 | 0.19 | 3.3 |
| | C3D | 44.31 | — | — |
| 11DA | | 106.11 | 0.55 | 5.5 |
| | 11D | 106.72 | — | — |
| 1814DA | | 177.04 | 0.65 | 5.1 |
| | 1814D | 178.39 | — | — |
| 21UA | | 180.17 | 0.47 | 4.2 |
| 28G6DA | | 259.07 | 0.65 | 6.6 |
| | 28G6D | 259.64 | — | — |
| 28REFUA | | 263.32 | 0.44 | 4.1 |
| 38DA | | 339.58 | 0.68 | 4.1 |
| | 38G5U | 341.60 | — | — |
| 48DA | | 419.08 | 0.88 | 4.6 |
| | 48G5U | 421.11 | — | — |
| 51UA | | 423.65 | 0.84 | 5.1 |
| | 57G7U | 498.01 | — | — |
| 584D | | 499.94 | — | — |

accelerate the positrons up to an energy of 1.1 GeV at second beam switchyard (SY2) and the positron beam is injected into a new damping ring (DR) [8] through the linac-to-DR transport line (LTR) [9]. The positron beams shall subsequently be transported back through the DR-to-linac transport line (RTL) to the SY2, and again accelerated up to 4.0 GeV in the linac for injection into the SKEKB LER, while the electron beams can be directly accelerated up to 7 GeV in the linac for injection into the SKEKB HER through the 180° arc section where the beam energy is

1.5 GeV.

LASER-BASED ALIGNMENT SYSTEM

Two independent laser-based alignment systems are available. One is for the alignment of the AB straight section, and the other is for that of the C5 straight section (see Fig. 1). The lengths of the laser-based fiducial lines are 132 m and 500 m for the AB and C5 straight sections, respectively. Two laser sources with commercially available 1-mW and 10-mW He-Ne lasers are installed along with the input optical system for the AB and C5 straight sections, respectively. Here, only the alignment system for the C5 straight section is described because the system is very similar between the AB and C5 straight sections.

The laser source is 16 m upstream from the upstream end face of unit C-1. The laser passes through laser pipes in vacuum while the laser source is installed in an atmospheric environment. The inner surface of the laser pipe is coated with a black paint composed of acrylic resin in order to prevent any unnecessary reflection and scattering of the laser light.

The laser pipes are evacuated using two scroll pumps with a pumping speed of 1000 l/min, which are installed 178 m and 321 m downstream from the input optical system. Two vacuum windows (thickness: 20 mm and 15 mm) made out of transparent synthetic quartz have been attached to the end faces of the initial and final (or first and last) laser pipes of the straight section to maintain vacuum higher in the laser pipes. A vacuum level of a few Pa can be attained. The propagation and stability characteristics of the laser fiducial along with the optical system are described in detail elsewhere [10].

A holder is precisely connected to both ends of the accelerator unit through a vacuum flange; a QPD with silicon semiconductor (diameter: 10 mm) is mounted at the center of the holder. The fifty accelerator units, with both regular and irregular lengths, are distributed along the C5 straight section; these units must be aligned with more than one

hundred QPDs in total within the transverse displacements of 0.1 mm in one standard deviation along the laser-based fiducial.

There are two fiducial points, which specify the transverse coordinates with respect to the laser axis. They are the transverse central positions of the initial and last QPDs (QPD_REF1UA and QPD_584D, respectively) installed at $z=6.3$ m and $z=500$ m downstream from the input optical system, respectively. These two fiducial QPDs are rigidly fixed at the floor of the accelerator tunnel after they have been locally aligned with a conventional laser tracker.

The transverse positions of the laser axis at the initial QPD is manually adjusted by translating the laser beam at the input optical system with the parallel plate in order to correspond to the center of the initial QPD, while the pointing of the laser beam is stabilized at the last QPD by controlling the x and y injection angles at the input optical system based on a feedback control [10].

The initial alignment of the accelerator units was carried out at the locations of QPDs. Each QPD can be manually (or remotely only one part) inserted into the center of the laser pipe. The transverse displacements of both the end surfaces of the accelerator unit can be determined with respect to the laser axis by analyzing the signal readouts from the QPD. Such a series of measurements provides an accurate view in the high-precision alignment of long linacs.

REAL-TIME MEASUREMENT ON DYNAMIC FLOOR MOTION

Long-term variations of the displacement vectors

The x and y ingredients of the displacements of accelerator components in rectangular coordinates are usually independently analyzed in time-series data. It is, however, important in the analyses to directly take into account the displacement vector instead of the use of the x (or y) ingredient because no special directivity may be provided in the direction of the displacement vector due to ground motion. Fig. 2 shows a typical example in the time series of the displacement vector obtained for QPD_38DA. It can be seen that the displacement vector has smoothly moved around the laser axis in the time direction. This is the reason why it is advantageous to the analysis with the displacement vectors in order to evaluate the transverse motion.

Figure 3 shows the time traces of the norm and phase in the displacement vectors measured for the accelerator units (or tunnel floor) at multiple locations with the remote-controllable QPDs during a nearly six-month period beginning on 7 January 2016. During the term the end positions of the laser axis were sufficiently stabilized to the center of the last QPD with the feedback control on. Here, it should be noted that the data are represented as the amount of variation in the displacement vectors, that is, the differentials from the corresponding initial data.

It can be understood that the norms of the displacement vectors monotonically increase except for that of QPD_REF1UA, which is nearest to the laser source. On

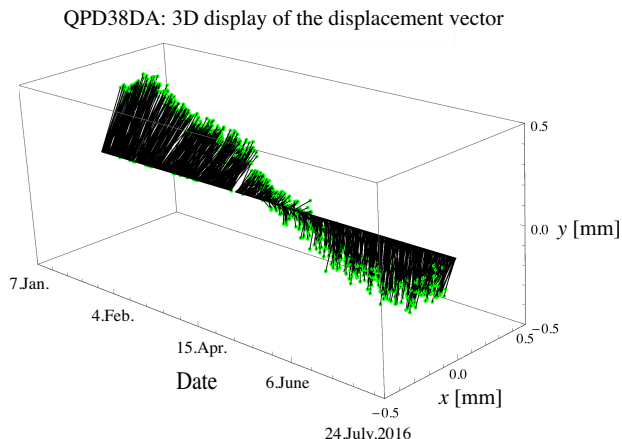


Figure 2: Variations in the time trace of the displacement vector obtained for the accelerator units (QPD_38DA) with the feedback control on.

the other hand, it can be seen that there are some incomprehensible fine structures in each time trace. The variations in the maximum norm (r_m) of the displacement vector in each time trace as a function of the QPD location are shown in Table 1. The maximum norms are spread over a range of 0.19–0.88 mm depending on the QPD location, and the average maximum norm ($\langle r_m \rangle$) is 0.65 mm except for that of QPD_REF1UA. The variations in the maximum growth rates (s_r) in the time traces as a function of the QPD location are shown in Table 1. The maximum growth rates of the norms are spread over a range of 3.3–6.6 $\mu\text{m}/\text{day}$ depending on the QPD location, and the average maximum growth rate ($\langle s_r \rangle$) is 4.9 $\mu\text{m}/\text{day}$ except for that of QPD_REF1UA.

It can also be found that the variations in the phase angle of the displacement vector in each time trace approach almost constant value since the middle of May 2016, while it can be seen that there are some steep variations until the end of March depending on the QPD location. Here, it should be noted that stepwise variations of the phase in the time traces normally arise in the phase region of 0 over 2π because the phase is defined by an angular range of 0– 2π . However, it can be clearly seen that relatively large stepwise jump arises on 28 January 2016 in the time traces of the phase for QPD_1814DA and QPD_28REFUA. It takes about four days in the rise time of the jump, and on the other hand, in the variations in the norms of the displacement vector during the corresponding term are less than 0.2 mm. It could be understood that during the corresponding term the displacement vector of the accelerator unit has rotated rather than increased in the transverse plane. Based on such vector representation in the displacement vector in polar coordinates, for the first time, complex and dynamic behavior of the tunnel floor could be seen much more clearly than the previous analysis.

The 500-m-long linac building comprises two floors, which together constitute the klystron gallery and tunnel in ground and underground floor, respectively. The linac

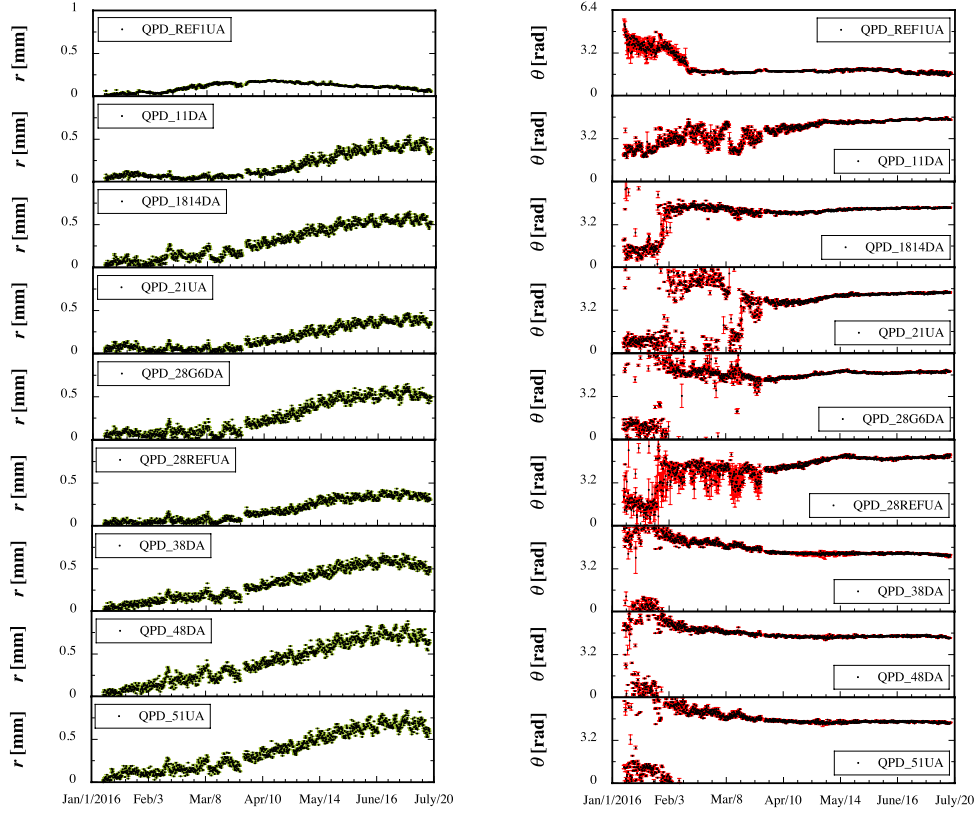


Figure 3: Time traces in (a) the norm and (b) phase angle of the displacement vector for the accelerator units (or tunnel floor) measured by the remote-controllable QPDs.

building comprises eight building blocks which are joined to be linearly aligned with seven expansion joints, which can absorb certain amount of elastic deformation due to expansion or contraction of the building blocks. However, the residual stress may induce some elastic deformation for the building blocks themselves. This mechanism may also contribute to the displacement of the accelerator units along the tunnel.

Last but not least, it should be noted that the two fiducial points to define the laser axis could also move dynamically. Thus, the laser axis itself could not become an entirely fixed and stable fiducial axis as an absolute fiducial line.

Cross-correlation analysis among the displacement vectors

It is generally valid to apply cross-correlation analyses in order to capture features in their mutual relations between different multivariate vector variables [11]. Based on the cross-correlation analyses in time traces of the displacement vectors, the variations in a cross-correlation function can be obtained in real time. This is one of powerful analysis methods to understand not only localized displacements of the accelerator units but also structural deformation of the building blocks along the entire length of the linac tunnel.

A cross-correlation function ($\hat{R}_k(i, j)$) between the n -th

displacement vectors ($\vec{d}_n(i)$ and $\vec{d}_n(j)$) obtained for the i -th and j -th QPDs, respectively, in time series with time lag of k is defined by

$$\langle \vec{\mu}(i) \rangle = \frac{1}{N} \sum_{n=1}^N \vec{d}_n(i), \quad (1)$$

$$\hat{C}_k(i, j) = \frac{1}{N} \sum_{n=k+1}^N (\vec{d}_n(i) - \langle \vec{\mu}(i) \rangle) \cdot (\vec{d}_{n-k}(j) - \langle \vec{\mu}(j) \rangle), \quad (2)$$

$$\hat{R}_k(i, j) = \frac{\hat{C}_k(i, j)}{\sqrt{\hat{C}_0(i, i)\hat{C}_0(j, j)}}. \quad (3)$$

Here, the dot in eq. (2) indicates the inner product for the displacement vectors, and $\langle \vec{\mu}(i) \rangle$ is the average of the i -th displacement vector in time series with a maximum data length of N , and $\hat{C}_k(i, j)$ is the cross-covariance function, which is similarly defined to the cross-correlation function. It should be noted that $\hat{R}_k(i, j)$ is normalized by using the cross-covariance functions, $\hat{C}_0(i, i)$ and $\hat{C}_0(j, j)$ for the i -th and j -th QPDs, respectively, without any time lag, $k=0$. Thus, $\hat{R}_k(i, j)=1$ (-1) shows strong positive (negative) correlation, and $\hat{R}_k(i, j)=0$ shows no correlation, and $\hat{R}_k(i, j)$ at $k=0$ ($k \neq 0$) stands for the cross-correlation function at present (past) time.

Figure 4 shows the time traces in the cross-correlation

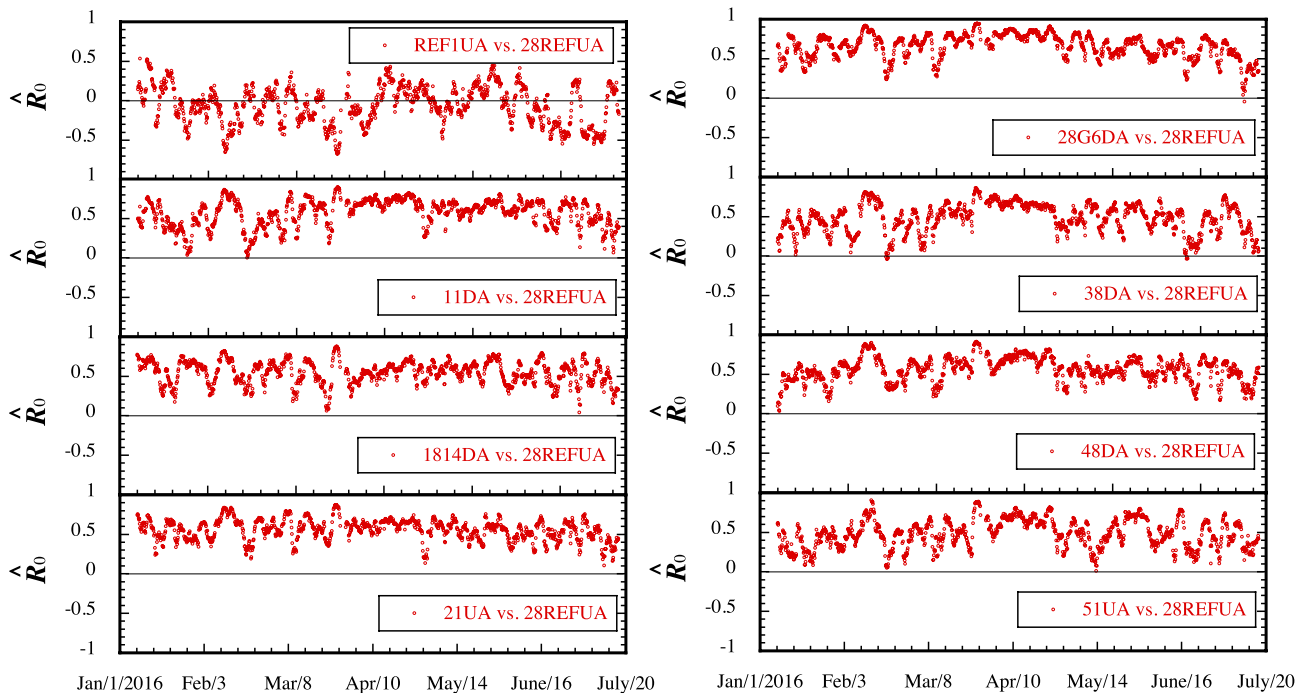


Figure 4: Time traces in the cross-correlation function of the displacement vectors between the reference QPD (QPD_REF28DA) and other QPDs.

function ($k=0$) of the displacement vectors for other QPDs to the reference QPD (QPD_REF28DA). Here, QPD_REF28DA is located almost at the middle location in the injector linac.

It can be seen that each cross-correlation function varies irregularly in the corresponding time trace, and however, the averages in the time traces decrease in the range of $\hat{R}_0=0.67$ to 0.48 in accordance with the distance from the reference QPD except for QPD_REF1UA where $\hat{R}_0=0.06$. This means that the relatively strong positive cross-correlations show averagely high coherency in dynamic displacements of the accelerator units along the entire length of the linac tunnel except for QPD_REF1UA. In other words, the results show that the floor level even at the expansion joints in each building block moves coherently on average with each other.

It should be noted that the time trace in the cross-correlation function for QPD_REF1UA is markedly different from those in the other cross-correlation functions. It may come from that the floor for the laser source is structurally separated from the tunnel floor of the building block [10]. It seems for QPD_REF1UA to stand alone from the other building blocks.

The cross-correlation functions for all the QPDs obtained at two different instantaneous dates are shown in Fig. 5. Here, those on a straight line tilted at 45 degree passing through the axis origin are the self-correlation function, and it becomes $\hat{R}_0=1$ by definition. Figure 5 (a) shows that the intensity distribution pattern obtained on 15 February 2016 at 0:00 am shows strong coherency, while Fig. 5 (b) obtained on 27 February 2016 at 8:00 am shows less

coherency. It should be noted that the cross-correlation function to QPD_REF1UA ($z=1.74$ m) show much less coherency because of the isolated behavior of QPD_REF1UA.

Though the analysis of the displacement vectors using the cross-correlation technique shows complicated features, some important features can be seen and it will be effective for the further analysis to understand the floor movement along the linac as a whole.

CONCLUSIONS

A new remote-controllable sensing system in a laser-based alignment system has been developed to measure slow dynamic displacements of the tunnel floor of the KEKB injector linac in real time. Based on the real-time measurements with the new system, we have observed non-negligible floor displacements due to dynamic ground motion during a nearly six-month period beginning on 7 January 2016.

The cross-correlation analysis on the floor displacements over the entire length of the linac tunnel was performed with the same data. Based on the analyses in the time traces of the displacement vectors, it can be seen that the cross-correlation functions vary irregularly in the corresponding time traces. However, the transverse positions of the floor measured at the remote-controllable QPDs moves coherently on average with each other. Such real-time measurements in dynamic motion of the tunnel floor along the entire length of the linac could help realize the stable operation of the injector linac.

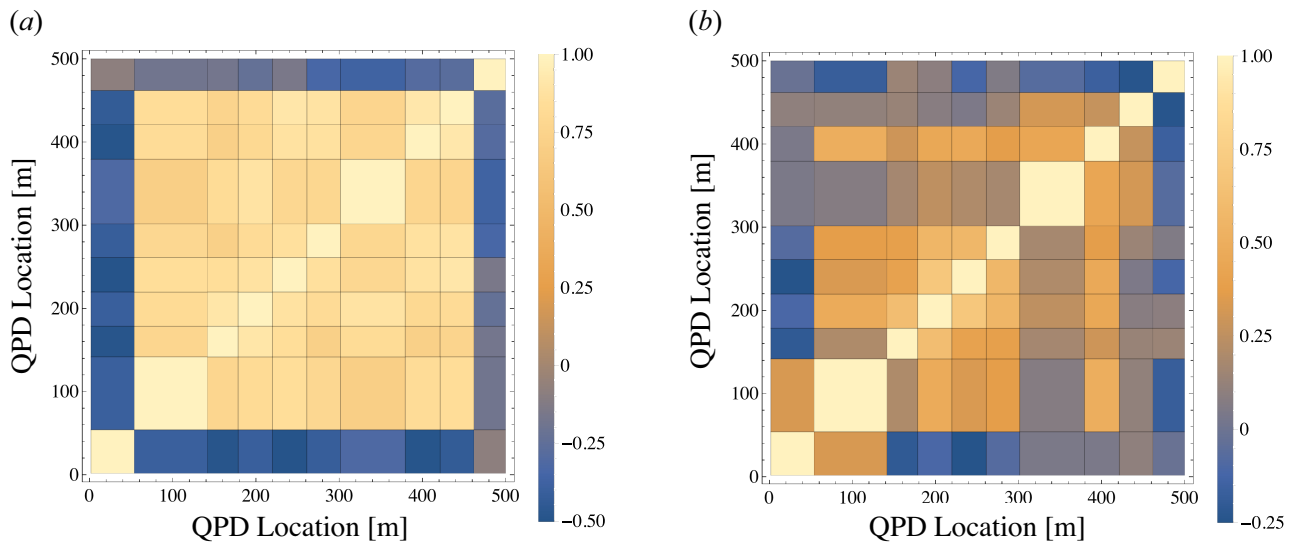


Figure 5: Intensity distributions of the cross-correlation function among all the QPDs in the displacement vector measurements along the C5 straight section obtained on (a) 15 February 2016 at 0:00 am and (b) 27 February 2016 at 8:00 am. The intensity distribution pattern is linearly encoded by the color scale, where bright yellow (dark blue) represents \hat{R}_0 maximum (minimum) value.

ACKNOWLEDGMENT

The authors would like to thank Prof. K. Furukawa of Accelerator Laboratory of KEK for his continuous supports on this work. They also thank Mrs. T. Kudou and Y. Mizukawa of Mitsubishi Electric System & Service Co., Ltd., who helped to conduct this work.

REFERENCES

- [1] Y. Ohnishi, *et al.*, Prog. Theor. Exp. Phys. (2013) 03A011.
- [2] T. Abe, *et al.*, Prog. Theor. Exp. Phys. (2013) 03A001.
- [3] T. Abe, *et al.*, KEK Report 2010-1, edited by Z. Doležal and S. Uno.
- [4] T. Suwada, *et al.*, to be submitted in Phys. Rev. Special Topics: Accelerators and Beams.
- [5] M. Akemoto, *et al.*, Prog. Theor. Exp. Phys. (2013) 03A002.
- [6] I. Abe, *et al.*, Nucl. Instrum. Methods Phys. Res. A **499**, 167-190 (2003).
- [7] T. Kamitani, *et al.*, Proceedings of the XXVth International Linac Conference (LINAC10), Tsukuba, Japan, 2010, pp.70-72.
- [8] M. Kikuchi, *et al.*, Proceedings of the 2nd International Particle Accelerator Conference (IPAC10), Kyoto, Japan, 2010, pp. 1641-1643.
- [9] N. Iida, *et al.*, Proceedings of the 2nd International Particle Accelerator Conference (IPAC11), San Sebastian, Spain, 2011, pp. 2857-2861.
- [10] T. Suwada, M. Satoh, S. Telada, and K. Minoshima, Rev. Sci. Instrum. 83, 053301 (2012).
- [11] G. Kitagawa, Introduction to Time Series Modeling, Monographs on Statistics & Applied Probability 114 (Chapman & Hall/CRC Press, New York, 2010), p. 17.